Direct numerical simulation of the turbulent channel flow of a polymer solution

R. Sureshkumar, Antony N. Beris, and Robert A. Handler

Citation: Physics of Fluids (1994-present) **9**, 743 (1997); doi: 10.1063/1.869229
View online: http://dx.doi.org/10.1063/1.869229
View Table of Contents: http://scitation.aip.org/content/aip/journal/pof2/9/3?ver=pdfcov
Published by the AIP Publishing

Direct numerical simulation of the turbulent channel flow of a polymer solution

R. Sureshkumar and Antony N. Beris[a)]
Department of Chemical Engineering, University of Delaware, Newark, Delaware 19716

Robert A. Handler
Naval Research Laboratory, Washington, D.C. 20375

(Received 29 May 1996; accepted 5 November 1996)

In this work, we present from first principles a direct numerical simulation (DNS) of a fully turbulent channel flow of a dilute polymer solution. The polymer chains are modeled as finitely extensible and elastic dumbbells. The simulation algorithm is based on a semi-implicit, time-splitting technique which uses spectral approximations in the spatial coordinates. The computations are carried out on a CRAY T3D parallel computer. The simulations are carried out under fully turbulent conditions albeit, due to computational constraints, not at as high Reynolds number as that usually encountered in polymer-induced drag reduction experiments. In order to compensate for the lower Reynolds number, we simulate more elastic fluids than the ones encountered in drag reduction experiments resulting in Weissenberg numbers (a dimensionless number characterizing the flow elasticity) of similar magnitude. The simulations show that the polymer induces several changes in the turbulent flow characteristics, all of them consistent with available experimental results. In particular, we have observed, associated with drag reduction, a decrease in the streamwise vorticity fluctuations and an increase in the average spacing between the streamwise streaks of low speed fluid within the buffer layer. These findings suggest a partial inhibition of turbulence generating events within the buffer layer by the macromolecules after the onset of drag reduction. This inhibition is further shown to be associated with an enhanced effective viscosity attributed to the extensional thickening properties of polymer solutions, as proposed in the past by Metzner, Lumley and other investigators. Using the simulation results obtained for different sets of parameter values which modify the relaxational and extensional properties of the model, we propose a set of criteria for the onset of drag reduction. © *1997 American Institute of Physics.* [S1070-6631(97)02003-5]

I. INTRODUCTION

The announcement in 1949[1] that the dissolution of minute quantities of high molecular weight linear chain polymers in a Newtonian solvent in a turbulent pipe flow can effect up to 70% reduction of the turbulent drag has triggered a vast research effort resulting in its large scale applications in fluid transportation.[2–5] In the late 1960s, experimental flow visualization techniques[6–9] were used to probe the structure of a Newtonian turbulent boundary layer, explaining its prominent role in the generation of turbulence in a pipe/channel flow. Similar experimental studies were conducted in later years for drag reduced turbulent flows to examine the modification of the wall layer and the ''events'' responsible for the production of turbulence by the polymer additive.[10–19] Earlier, rheological studies were initiated on drag-reducing polymer systems to investigate the effects of polymer extensibility and relaxation on the onset and the extent of drag reduction.[20–25] Significant modification of turbulence statistics associated with approximately 30% drag reduction has been reported even at 1–2 ppm polymer concentrations in the flow.[26]

The available experimental information has been used in developing theoretical ideas for the mechanisms of drag reduction. These mechanisms can be related to the modification of the solvent rheology by the polymer additive: This results in a viscoelastic fluid, with properties intermediate to those of a viscous fluid and an elastic solid, possessing a partial memory characterized by a relaxation time. Viscoelastic flows are distinguished from viscous flows by the existence of non-zero normal stress differences in a simple shear flow and an apparent variable viscosity which typically decreases in shear flows and increases, often by several orders of magnitude, in extensional flows. Viscoelastic fluids also exhibit recoil upon flow cessation due to memory effects.[27,28] Hence, the proposed mechanisms of drag reduction are typically based on the enhanced macromolecular resistance to extensional motions[2,3,20–24] or elastic memory/relaxational effects.[25,29–32] However, the details are sketchy and direct evidence for any specific mechanism is still lacking.

Direct numerical simulations of turbulent flows (DNS) have become possible with the development of accurate and efficient spectral methods and the wider availability of high performance vector and parallel supercomputers.[33–36] In particular, for turbulent channel flow, DNS has not only confirmed the established picture of wall bounded turbulence[37] but has also allowed a detailed evaluation of its structural and statistical features.[38,39]

The application of DNS to the direct demonstration of the drag reduction phenomenon was recently addressed by

a)Author to whom all correspondence should be addressed.

 1070-6631/97/9(3)/743/13/$10.00

Handler *et al.*[40] who showed that assigning random phase shifts to the long wavelength Fourier components of the velocity at prescribed time intervals in an otherwise Newtonian turbulent channel flow results in a drag-reduced turbulent flow. That work was based on the observation that flow could be decomposed into non-propagating and propagating (wave-like) modes.[41,42]

More recently, the role of an enhanced elongational viscosity on drag reduction was investigated numerically utilizing generalized Newtonian models in turbulent pipe[43,44] and channel flow.[45] Although the interpretation of the results is hindered from the fact that to accommodate a variable phenomenological viscosity low order accuracy (finite-difference) methods were used, there is significant evidence provided that an enhanced, preferably anisotropic, extensional viscosity can lead to a drag-reduced flow. Depending on the details of the phenomenological models used, those simulations were able to capture qualitatively several effects observed experimentally, such as the upward shift in the logarithmic region of the mean flow profile, enhanced axial velocity fluctuations and decreased radial/wall-normal velocity fluctuations.[43,45] However, due to the purely viscous nature of the models used which do not account for any relaxational or fading memory effects, it was not possible to investigate the onset phenomenon. Significant evidence has been provided by these works[43,45] on the critical role of an enhanced extensional viscosity of a polymer solution in promoting drag reduction. However, obtaining conclusive evidence for the drag reduction phenomenon through direct numerical simulations using an independently evaluated microscopic model developed from first principles has remained elusive so far.

Previous theoretical works based on an Oldroyd-B type viscoelastic constitutive equation have only addressed the influence of elasticity on the stability of the channel flow against infinitesimally small perturbations[46,47] and the uncoupled problem, i.e., to solve for the polymer chain conformation with a given turbulent flow field.[48] Early attempts at a DNS of the fully coupled turbulent viscoelastic flow using models which can be derived from first (kinetic theory) principles were unsuccessful primarily because of instabilities which developed in the numerical time-integration of the additional stress or conformation variables which need to be introduced in order to describe the relaxational phenomenon.[49] It is only recently that these numerical stability issues have been at least partially resolved through the introduction of a small, controlled amount of numerical diffusivity to the evolution equation for the polymer chain conformation tensor.[50,51] We utilize here those same techniques to provide DNS of a viscoelastic turbulent channel flow.

The model used in this work is the FENE-P (finitely extensible nonlinear elastic-Peterlin) dumbbell model. It has been extensively used in the past to correlate experimental data for various dynamic properties of polymer solutions, such as the shear and extensional viscosity, transients and normal stress differences.[27,28,52] Moreover, the suitability of nonlinear dumbbell models in describing the polymer conformation in turbulent flows has been suggested in the past, see Ref. 53 for a detailed discussion. In the FENE-P model, the conformational details of the macromolecule are described macroscopically by a conformation tensor, $\tilde{\mathbf{c}} \equiv \langle \tilde{\mathbf{q}}\tilde{\mathbf{q}} \rangle$, where $\tilde{\mathbf{q}}$ denotes the instantaneous end-to-end connector vector of the dumbbell and the angular brackets represent an ensemble average over all possible realizations. By definition, $\tilde{\mathbf{c}}$ is symmetric and positive definite and it is easy to verify that the invariants of $\tilde{\mathbf{c}}$ are objective, i.e., reference frame-invariant, measures. The model parameters are the relaxation time, λ, of the dumbbell and a maximum allowable root mean square extension of the dumbbell, L. An obvious computational complexity which arise in the DNS using such models arise from the additional six variables, i.e., six independent components of $\tilde{\mathbf{c}}$, which have to be solved for at each time step along with the velocity and pressure. We have addressed this issue by resorting to parallelization of the spectral algorithm on a CRAY-T3D platform.[54]

This paper is organized as follows. In Sec. II, we provide the governing equations and define dimensionless parameters. In Sec. III, we briefly describe the numerical method and define the simulation conditions. In Secs. IV A–IV C, we discuss our simulation results. Our concluding remarks are offered in Sec. V.

II. GOVERNING EQUATIONS AND MODEL PARAMETERS

In an orthogonal Cartesian coordinate system, we chose the x axis as the mean flow direction, i.e., the direction of the constant, externally imposed, pressure gradient and the y and the z axes as the wall-normal and spanwise directions respectively. Let ν_0 denote the zero-shear kinematic diffusivity of the polymer solution, defined as the ratio of total zero-shear viscosity η_0, to the density ρ. We choose the friction velocity U_τ, defined as $U_\tau = \sqrt{\tau_w/\rho}$, where τ_w represents the shear stress at the wall as a velocity scale, ν_0/U_τ as a length scale and ν_0/U_τ^2 as a time scale. The conservation equation for momentum for a general incompressible viscoelastic fluid can then be written in dimensionless form as

$$\frac{\partial \tilde{\mathbf{v}}}{\partial t} + \tilde{\mathbf{v}} \cdot \boldsymbol{\nabla} \tilde{\mathbf{v}} = -\boldsymbol{\nabla} \tilde{p} + [\beta \nabla^2 \tilde{\mathbf{v}} + (1-\beta) \boldsymbol{\nabla} \cdot \tilde{\mathbf{s}}] + \frac{1}{\mathrm{Re}_\tau} \hat{e}_x, \tag{1}$$

where $\tilde{\mathbf{v}}$, $\tilde{p}$ and $\tilde{\mathbf{s}}$ denote the velocity, the excess pressure and the viscoelastic contribution to the total stress, respectively. The scale for pressure in Eq. (1) is simply the wall shear stress, τ_w. The last term in Eq. (1) represents the constant, mean pressure drop per unit length across the channel which in the dimensionless units used here is equal to the inverse of the friction Reynolds number, Re_τ, defined as $\mathrm{Re}_\tau = hU_\tau/\nu_0$, where h is the channel half-width. The parameter β appearing in Eq. (1) represents the ratio of the solvent (η_s) to the total zero-shear rate solution viscosity, η_0. Also notice that in Eq. (1) the viscoelastic stress tensor, $\tilde{\mathbf{s}}$ is made dimensionless using the viscous units $\eta_{p0} U_\tau^2/\nu_0$, where η_{p0} $(=\eta_0 - \eta_s)$ is the polymer contribution to the total zero-shear solution viscosity.

In addition to Eq. (1), we need to supply a constitutive relationship for the polymeric stress tensor, $\tilde{\mathbf{s}}$. We have chosen in this work the FENE-P (finitely extensible nonlinear elastic-Peterlin) model which is based on a dumbbell de-

scription of a polymer chain of two equal masses connected by a finitely extensible entropic spring.[52,55] In this model, the viscoelastic stress is related to the departure of the conformation tensor $\tilde{\mathbf{c}}$, characterizing the average second moment of the polymer chain end-to-end distance vector, from its equilibrium unit isotropic tensor state **1**, as

$$\tilde{\mathbf{s}} = \frac{\tilde{f}(\tilde{r})\tilde{\mathbf{c}} - \mathbf{1}}{\mathrm{We}_\tau}, \tag{2}$$

where We_τ is the Weissenberg number defined as the product of the polymer relaxation time and a characteristic shear rate, i.e., $\mathrm{We}_\tau = \lambda U_\tau^2 / \nu_0$. In Eq. (2), $\tilde{\mathbf{c}}$ is made dimensionless with respect to $k_B T/H$, where k_B, T and H denote the Boltzmann constant, the absolute temperature and the dumbbell spring constant, respectively. The function $\tilde{f}(\tilde{r})$, known as the Peterlin function,[56] is defined as

$$\tilde{f}(\tilde{r}) = \frac{L^2 - 3}{L^2 - \tilde{r}^2}, \tag{3}$$

with $\tilde{r}$ representing the root mean square chain extension, i.e., $\tilde{r}^2 = \mathrm{trace}(\tilde{\mathbf{c}})$. As evident from Eq. (3), the Peterlin function limits the chain extension to a maximum value L, since as $\tilde{r}$ approaches L, the force required for further extension approaches infinity.

The evolution equation for the conformation tensor $\tilde{\mathbf{c}}$, is derived using the principles of kinetic theory[28,52,55] to describe the chain relaxation dynamics as

$$\frac{\partial \tilde{\mathbf{c}}}{\partial t} + \tilde{\mathbf{v}} \cdot (\boldsymbol{\nabla} \tilde{\mathbf{c}}) - [\tilde{\mathbf{c}} \cdot (\boldsymbol{\nabla} \tilde{\mathbf{v}}) + (\boldsymbol{\nabla} \tilde{\mathbf{v}})^\dagger \cdot \tilde{\mathbf{c}}] = -\frac{\tilde{f}(\tilde{r})\tilde{\mathbf{c}} - \mathbf{1}}{\mathrm{We}_\tau}. \tag{4}$$

Note that Eq. (4) represents a tensorial generalization of a traditional relaxation model with the left hand side corresponding to a materially objective time derivative for $\tilde{\mathbf{c}}$ and the right hand side being proportional to the departure of $\tilde{\mathbf{c}}$ [weighted with $f(\tilde{r})$] from its equilibrium value. Equations (1)–(4) along with the no-slip $\tilde{\mathbf{v}} = 0$ boundary conditions for the velocity on the channel walls, constitute the governing equations for the viscoelastic channel flow which are subsequently solved numerically.

The time-average and the fluctuations associated with any flow variable, say $\tilde{q}$, (where q could be **v**, p, **c** or **s**) would be denoted by Q and q, respectively. Moreover, we let $\tilde{\mathbf{v}} = (\tilde{u}, \tilde{v}, \tilde{w})$ where $\tilde{u}$, $\tilde{v}$ and $\tilde{w}$ denote the velocities in the x, y and z directions. Notice that $\mathbf{V} = (U(y), 0, 0)$.

III. NUMERICAL ALGORITHM AND SIMULATION CONDITIONS

The numerical algorithm used for the time-integration of the governing equations outlined in the previous section, Eqs. (1)–(4), was developed by Beris and Sureshkumar in an earlier work,[50] based on the semi-implicit, time-splitting, spectral simulation techniques which have been successfully employed before in the DNS of Newtonian channel flow.[33,34,38] The simulations are carried out in a unit cell of dimensions $10h \times 2h \times 5h$ in the x, y and z directions, respectively. The spanwise (z) dimension is approximately equal to six times the average spacing between the streamwise streaks for the Newtonian flow. The streamwise (x) dimension of the unit cell is chosen to be the largest to capture the fairly elongated quasi-streamwise vortical structures.[57] As explained in detail in our previous work, it was necessary, in order to ascertain a stable numerical integration of the evolution equation for the conformation tensor, to introduce into Eq. (4), an artificial stress diffusive term, $(\kappa/\nu_0)\boldsymbol{\nabla}^2 \tilde{\mathbf{c}}$, where κ denotes a constant isotropic diffusivity.[51] In this case, the boundary conditions for the conformation tensor were supplied by integrating in time the original constitutive equation (without the artificial diffusivity) at the solid boundaries.[51]

In order to accommodate the significant computational requirements imposed by the additional variables (as compared to the Newtonian case), we adapted the algorithm to a parallel computing environment (CRAY T3D), where the inherent 3D torus parallel architecture maps very well with the three-dimensional computational domain.[54] The algorithm requires approximately 1 s for the Newtonian and 3 s for the viscoelastic simulations per time step on 32 processors of the CRAY T3D, a performance comparable to that of a single processor CRAY C-90. The (dimensional) time-step size, Δt, used in the viscoelastic simulations is typically a factor of 5 smaller compared to that used in the Newtonian case where Δt of $10^{-3} h/u_\tau$ was used. Hence, for simulations over a given period of time, the viscoelastic simulations require approximately 15 times more CPU resources as compared to the Newtonian one.

As initial conditions for our viscoelastic calculations we used the velocity data corresponding to the fully turbulent Newtonian channel flow, realized at a friction Reynolds number $\mathrm{Re}_\tau = 125$, with a mean flow Reynolds number based on the channel half width Re_m, of 1840. Using these data, we further computed the average velocity $U(y)$ and under the assumption of a unidirectional shear flow with the velocity profile given by $U(y)$, we evaluated the conformation tensor components from Eq. (4). This procedure yields for the conformation tensor components evaluated using the mean shear flow assumption, $\mathbf{C}^{ss}$, the following results:

$$\begin{aligned}
\Omega(y) &= \frac{\sqrt{2}\mathrm{We}_\tau}{L}\frac{dU}{dy}, \\
F(y) &= \frac{\sqrt{3}\Omega(y)}{2\sinh(\phi/3)}, \\
C_{xx}^{ss} &= \frac{1}{F(y)}\left[1 + \frac{2\mathrm{We}_\tau^2}{F^2(y)}\left(\frac{dU}{dy}\right)^2\right], \\
C_{xy}^{ss} &= \frac{\mathrm{We}_\tau}{F^2(y)}\frac{dU}{dy}, \\
C_{yy}^{ss} &= C_{zz}^{ss} = \frac{1}{F(y)}, \\
C_{xz}^{ss} &= C_{yz}^{ss} = 0,
\end{aligned} \tag{5}$$

where $\phi = \sinh^{-1}(3\sqrt{3}\Omega/2)$. Using these results [Eq. (5)] as initial data for the $\tilde{\mathbf{c}}$ tensor components and the fully turbulent Newtonian velocity field as initial data for $\tilde{\mathbf{v}}$, the governing equations were integrated for a few thousand time steps with the parameter $\beta = 1$ (this decouples $\tilde{\mathbf{v}}$ and $\tilde{\mathbf{c}}$) until

stationary data were obtained for $\tilde{\mathbf{c}}$. The data obtained for $\tilde{\mathbf{v}}$ and $\tilde{\mathbf{c}}$ from these calculations were subsequently used to initiate the simulations using the fully coupled (i.e., $\beta \neq 1$) system of equations until a stationary state was achieved. The stationary state thus eventually achieved is characterized by the satisfaction of the overall force balance across the channel, i.e.,

$$\beta \frac{dU}{dy} + (1-\beta) S_{xy} - \overline{uv} = 1 - y/\mathrm{Re}_\tau . \tag{6}$$

Due to the computational constraints resulting from the required resolution to capture the dissipative length scales, we limited the investigations reported in this work to a friction Reynolds number $\mathrm{Re}_\tau = 125$. For this Reynolds number it has been shown[40] that for a Newtonian fluid a sustainable fully turbulent flow can be obtained corresponding to $\mathrm{Re}_m = 1840$. However, we need to emphasize that using dilute polymer solutions drag reduction has been observed experimentally at higher Reynolds numbers corresponding to $\mathrm{Re}_m \approx 8900$ or higher.[26] In order to compensate for the lower Reynolds number we have simulated the behavior of a fluid which is more elastic than the ones which have been so far used experimentally. This is primarily captured in the parameter β in Eq. (1) for which a value of 0.9 was selected for all our viscoelastic simulations. Moreover, the simulations were carried out for $L = 10$ and 2 and the Weissenberg numbers (We_τ) used in the calculations ranged from 12.5 to 50.

The simulations reported in this paper were performed with a $64(\text{in } x) \times 65(\text{in } y) \times 64(\text{in } z)$ with a stress diffusivity $\kappa/(U_\tau h) = 10^{-2}$. For a test of convergence against the numerical parameters certain results were also obtained with a finer ($128 \times 129 \times 128$) spatial discretization and a smaller value of $\kappa/(U_\tau h) = 5 \times 10^{-3}$. As discussed in detail in section 4.4, the results obtained using these two computational grids showed the same qualitative behavior and only minor quantitative differences.

IV. RESULTS AND DISCUSSION

A. The onset of drag reduction

In Fig. 1, we present the mean flow Reynolds number, Re_m, as a function of dimensionless time in units of h/U_τ, i.e., the abscissa in Fig. 1 is t/Re_τ, for a value of $L = 10$ at 4 different values of the Weissenberg number keeping the average pressure drop (i.e., wall friction) the same, i.e., $\mathrm{Re}_\tau = 125$. One unit of time in Fig. 1 corresponds to approximately 1.3 times a typical large eddy turn over time, evaluated as $2h/u_{\mathrm{rms,max}}$, for the simulated Newtonian flow. As can be seen from there, the simulations performed at $\mathrm{We}_\tau = 12.5$ did not show any perceptible changes in Re_m and thus in the mean mass flux through the channel. Similarly, we found no appreciable differences in the statistical features of turbulence. However, increasing We_τ to 25 resulted in a clear enhancement of Re_m, thereby indicating drag reduction. These observations suggest, consistent with experiments,[2] that the drag reduction phenomenon sets in abruptly once a critical value of the Weissenberg number, say We_c, is reached rather than presenting a gradual transition from the Newtonian results. We further increased We_τ to 37.5 and finally to 50, for which value we integrated the governing equations over a time of approximately $40h/U_\tau$ which translates to about 200 000 time-steps. As can be seen from Fig. 1, the viscoelastic simulation at $\mathrm{We}_\tau = 50$ approaches but it does not reach within the time span investigated here (see also pertinent comments in Sec. IV D) a statistically stationary turbulent flow state. Still it clearly shows drag reduction and sustainable turbulence. The Re_m corresponding to this flow realized at $\mathrm{We}_\tau = 50$, calculated between $t = 41h/U_\tau$ and $56h/U_\tau$, was found to be approximately 1994, indicating an enhancement of the flow by about 8.4% as compared to the Newtonian flow realized for the same wall friction, $\mathrm{Re}_\tau = 125$. This is equivalent to approximately 15% drag reduction under conditions of equal mass flux using the correlation of Dean.[58]

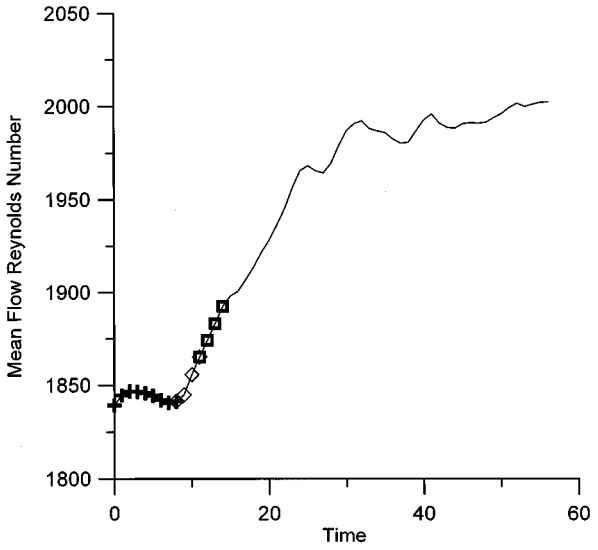

FIG. 1. The mean flow Reynolds number, Re_m, as a function of time in units of h/U_τ, for constant pressure drop corresponding to a wall friction given by $\mathrm{Re}_\tau = 125$. $\mathrm{We}_\tau = 12.5$ (+); 25 ($\diamond$); 37.5 ($\square$) and 50 (solid line).

The presence of a critical Weissenberg number has been stipulated in the past.[2,3,25,30] However, Lumley anticipated the critical relaxation time to be of the same order as the wall time scale ν/U_τ^2, i.e., the critical Weissenberg number (referred also to as the Deborah number in the literature) to be order 1. An accurate direct experimental verification of this hypothesis would be rather difficult especially for very dilute systems due to the uncertainties which would arise from the estimation of the relaxation time.[25] The experiments performed by Hershey and Zakin[25] present an $O(1)$ transition Weissenberg number for fairly concentrated systems ($>0.05\%$ by weight), but for a more dilute system (0.005% by weight, see Table 3 in Ref. 25) a We_c of 36 is reported. In our simulations, we present an onset Weissenberg number We_c between 12.5 and 25. In Sec. IV C, we present, based on our simulation results, a discussion of a possible mechanism of onset which requires the satisfaction of an extensional as well as a relaxational criterion for drag reduction to occur.

B. Comparison of the Newtonian and viscoelastic turbulence ($L=10$)

In order to obtain time-averaged statistics for the flow variables, a number of realizations obtained over time intervals much larger than a typical (dimensional) large eddy turnover time t_e, were used after a statistically stationary state has been established. For instance, averages were performed over time intervals of $40h/U_\tau$ and $15h/U_\tau$ for the Newtonian and viscoelastic cases respectively. Note that for the Newtonian turbulent flow simulated in this work, $t_e h/U_\tau \approx 1.3$.

One of the consequences of the addition of a polymer to a solvent is the introduction of a shear dependence to the (apparent) viscosity of the solution in simple shear flow. Indeed, typical viscoelastic fluids are ''shear thinning;'' i.e., their shear viscosity decreases as a function of shear rate, this decrease taking place after a critical value of the shear rate corresponding to a Weissenberg number of order one.[27] It is important to take the shear thinning effect into account in order to obtain proper wall scales so that the linear relationship $U(y)=y$ is satisfied in the viscous sublayer. This can be accomplished by rescaling the space coordinates using an effective kinematic viscosity so that it captures the contribution of the polymer stress at the wall. For the FENE-P model utilized here, this effective (wall) kinematic viscosity, ν was computed from the simulation data using the relationship

$$\frac{\nu}{\nu_0}=\frac{\beta\dfrac{dU}{dy}_{y=0}+(1-\beta)S_{xy,y=0}}{\dfrac{dU}{dy}_{y=0}}, \tag{7}$$

which in turn defines the renormalized distance from the wall, $y_e=\nu_0 y/\nu$. Hence, in the subsequent sections, whenever we present viscoelastic data vs distance from the wall, the abscissa should be understood as y_e, such that $0(\text{wall}) \leqslant y_e \leqslant \mathrm{Re}_\tau \nu_0/\nu(\text{center line}) \approx 135$ for $L=10$ and $\mathrm{We}_\tau=50$.

1. Mean velocity profiles

With the rescaling using the effective kinematic diffusivity defined by Eq. (7), the linear relationship $U=y$ is duly satisfied in the viscous sublayer close to the wall ($y<2$) as seen in Fig. 2. On the other hand, in the inertial sublayer far away from the wall ($y>50$), a logarithmic relationship is obtained. For the Newtonian flow, the logarithmic profile is approximately given by $U=2.5\ \ln(y)+5.5$. The simulation data slightly over-predict the Newtonian inertial profile due to the (low) finite Reynolds number used and this has been observed in previous Newtonian simulations as well.[40] It can also be seen from Fig. 2 that the viscoelastic inertial velocity profile can be correlated with $U=2.5\ \ln(y)+7$, implying an increment only in the intercept value as compared to the Newtonian case. As seen from Fig. 2, the higher value of the intercept in the viscoelastic case results in an increase in the thickness of the buffer layer, which is defined here as the value of y at which the extrapolated viscous and the inertial sublayer profiles intersect, as also observed in experiments.[26]

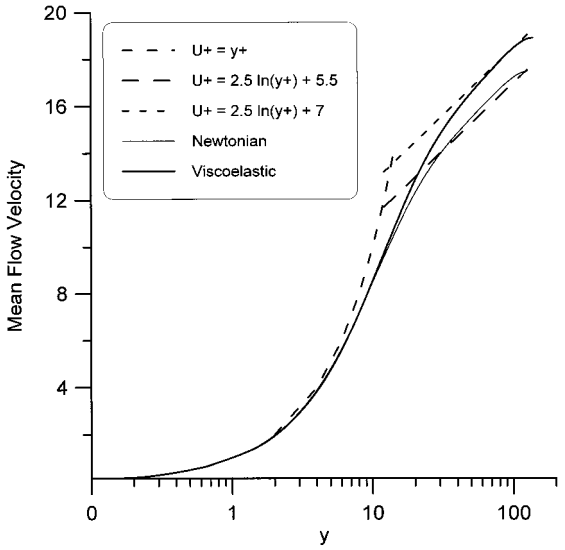

FIG. 2. The mean flow velocity, U, as a function of the distance from the wall, y. Also shown are the linear wall ($U=y$) and logarithmic inertial sublayer ($U=2.5\ \ln(y)+5.5$) asymptotes for the Newtonian flow and a logarithmic profile, $U=2.5\ \ln(y)+7$, to fit the viscoelastic inertial sublayer profile.

2. Velocity fluctuations and Reynolds shear stress

As can be seen from Fig. 3, the root mean square (rms) values for the velocity fluctuations in the viscoelastic flow, evaluated over the x and z directions as a function of y, are increased for the streamwise component u, and decreased for the wall-normal (v) and the spanwise (w) components as compared to the Newtonian results. Moreover, the location above the wall where u_{rms} attains a maximum shifts further into the bulk of the flow as compared to the Newtonian case. Both these findings have been experimentally associated with drag reduction even for very dilute (1–2 ppm) polymer

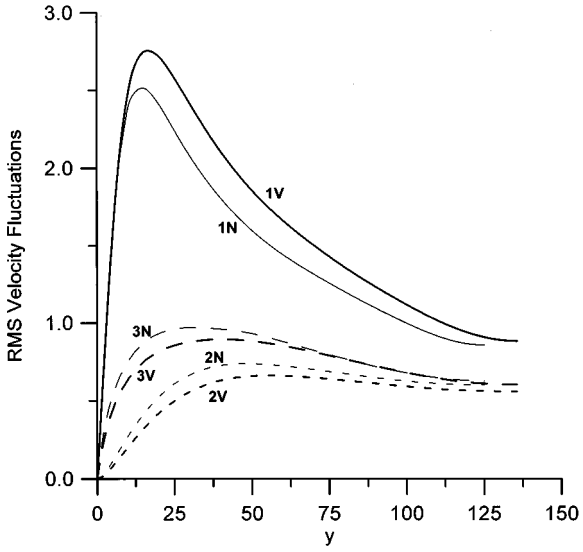

FIG. 3. The rms velocity fluctuations as a function of the distance from the wall. Curves 1N, 2N and 3N show the streamwise, the wall-normal and the spanwise components for the Newtonian flow, respectively; curves 1V, 2V and 3V show corresponding data for the viscoelastic flow.

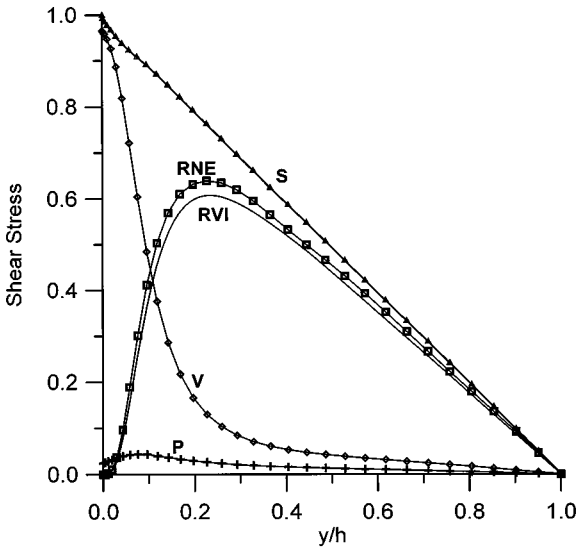

FIG. 4. The Reynolds shear stress for both the Newtonian (RNE) and the viscoelastic (RVI) flows. Also shown are the purely viscous (V) and the viscoelastic (P) contributions to the total shear stress and the total shear stress (S) in the viscoelastic flow.

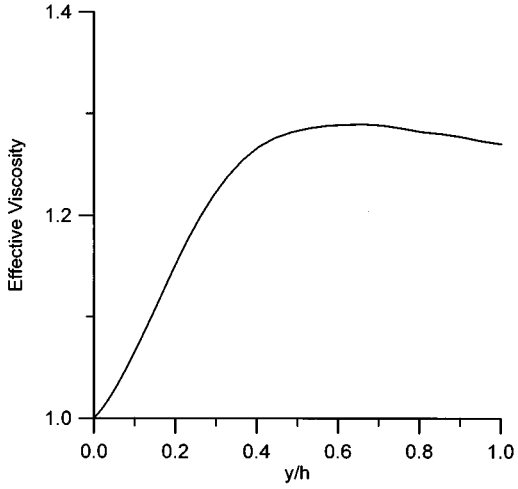

FIG. 5. The variable effective viscosity defined by Eq. 8, η_{eff}, as a function of y for $\text{We}_\tau = 50$.

solutions,[26] although because of experimental difficulties direct measurements of the fluctuations along the spanwise direction are not, to the best of our knowledge, available for the channel flow. However, experiments for the turbulent pipe flow have shown that the rms spanwise flutuations decrease when drag reduction occurs.[59] The observed increase of u_{rms} in the buffer layer and the shift in the maximum value can be explained by a scaling argument based on Prandtl's mixing length hypothesis, $u_{\text{rms}} \sim (dU/dy)y$, since $dU/dy = 1$ in the viscous sublayer for both the Newtonian and viscoelastic cases, and the viscous sublayer extends to higher y values for the latter.[3] The same argument can also explain the fact that u_{rms} for both the Newtonian and the viscoelastic cases approach the same values close to the centerline of the channel, as also seen in Fig. 3, since there both dU/dy and y (proportional to the largest possible eddy size) are the same for both the viscoelastic and Newtonian flows.

Figure 4 shows the various contributions to the mean shear stress as a function of the normalized wall distance. The mean total shear stress decreases linearly with y as a consequence of the momentum balance in the mean flow direction [Eq. (6)]. The total shear stress can be decomposed into its contributions from inertial (Reynolds shear stress), purely viscous and (for a viscoelastic fluid) viscoelastic forces. Because of the positive contribution of the latter (see curve P in Fig. 4) the Reynolds shear stress for the viscoelastic flow decreases as compared to that for the Newtonian one. This has also been observed in the experiments.[26,60] In a discussion of experimental observations made on $\overline{-uv}$ in drag reduced flows, Tiederman (see pp. 191–192 of Ref. 63) points out that in certain experiments the measured Reynolds shear stress and the direct viscous shear stress (arising from dU/dy) did not add up to yield a linear dependence on y. We believe this is due to the neglected viscoelastic contribution to the total shear stress S_{xy}, a quantity difficult to be measured for very dilute polymer systems.

The combination of the purely viscous and viscoelastic contributions to the stress, which based on the discussion above is equal to the total shear stress minus the Reynolds shear stress, can be described phenomenologically in terms of a *variable effective viscosity* η_{eff}, which is a function of y,[24,61] i.e.,

$$\eta_{\text{eff}}(y) = \frac{1 - y/\text{Re}_\tau - (-\overline{uv})}{dU/dy}. \tag{8}$$

It is of interest that the distribution of the streamwise vorticity in the flow has been correlated in the past with the functional dependence of η_{eff} on y, evaluated using experimental measurements for the Reynolds shear stress. For a fairly concentrated polymer solution, η_{eff} was found to increase within the viscous sublayer from the solvent viscosity value at the wall to about 4 times as much at the edge of the buffer layer. In Fig. 5, we present $\eta_{\text{eff}}(y)$ vs y for the drag-reduced flow realized at $\text{We}_\tau = 50$. It can be seen from there that $\eta_{\text{eff}}(y)$ shows a functional behavior qualitatively similar to the experimental one, albeit we find only a moderate increase in $\eta_{\text{eff}}(y)$ (30%) in the bulk of the flow as compared to its value at the wall.

3. Streamwise vorticity, spectra and streak spacing

In Fig. 6, we show, for the first time to our knowledge, the decrease in the intensity of the streamwise vorticity fluctuations made dimensionless with respect to U_τ/h, ω_x, accompanying drag reduction in a turbulent channel flow. The streamwise vorticity fluctuations for both the Newtonian and the viscoelastic flows show a characteristic minimum followed by a maximum. Their locations correspond to the average locations of the edge and the center, respectively, of the streamwise vortices (eddies) in the wall region.[38] As Fig. 6 shows, the introduction of the polymer not only reduces the intensity of the fluctuations but also shifts the locations of both the minimum and the maximum towards the bulk of the flow. This implies a reduction in the intensity of the wall eddies and an increase in their average size. The observed

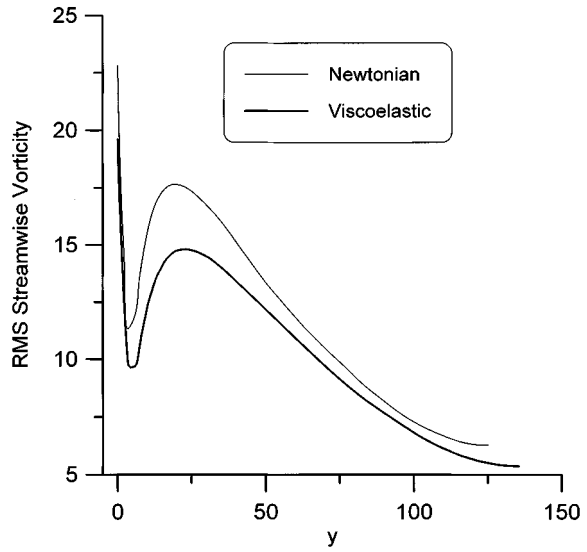

FIG. 6. The rms streamwise vorticity fluctuations, made dimensionless with respect to U_τ/h, as a function of y.

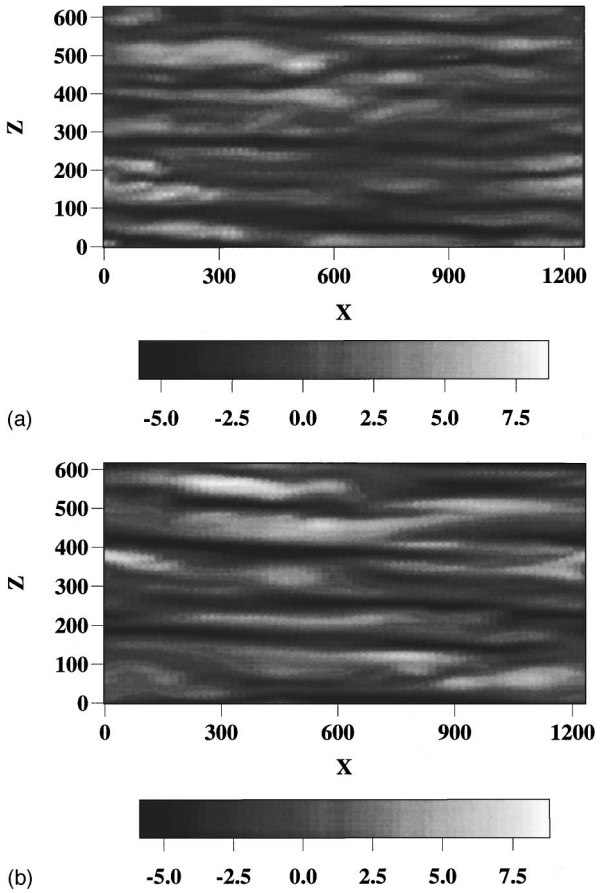

FIG. 7. Instantaneous snap shots of the streamwise fluctuating velocity in the $x-z$ plane at $y\approx 15$ for both the Newtonian (a) and the viscoelastic (b) flows. The dark and the light regions represent the low and high speed fluid, respectively. The increase in the spacing between the streamwise streaks of low speed fluid due to viscoelasticity can be seen by comparing a and b.

reduction in the intensity of the wall eddies, provides evidence for a mechanism of drag reduction based on the inhibition of the wall eddies since they facilitate significant amounts of the turbulence production. In flow visualizations large intermittent eddies were observed which grow by deriving energy from the mean shear, reach a peak activity and then decay gradually.[7,57,62] These mean flow oriented eddies were also shown to be responsible for ''sweeping'' slowly moving fluid from close to the wall, resulting in the generation of low speed streaks, a mechanism which eventually leads to the production of Reynolds stress.[9] The inhibition of the near-wall eddies in polymer solutions may be anticipated due to the enhanced resistance of the macromolecules in extensional flow and has been proposed as a possible mechanism of drag reduction in the past.[21–24]

The influence of elasticity on the streaky structures, i.e., the streamwise streaks of low speed fluid, is clearly seen in Fig. 7, where we present a gray scale representation of an instantaneous snapshot of the fluctuations in the streamwise velocity about its mean value in the $x-z$ plane both for the Newtonian and the viscoelastic flows. Figure 7 shows that the introduction of the polymer results both in an increase in streak spacing as well as an increase in the range of streamwise velocity fluctuations. These findings are consistent with those obtained using direct flow visualization techniques and through the evaluation of the one-dimensional energy spectrum.[10–19] These studies have shown an increase in the average streak spacing, Δ_s, associated with drag reduction and Tiederman[63] provides the correlation $\Delta_s = 1.9 \times$percentage drag reduction. Furthermore, for dilute solutions, the percentage increase in the streak spacing has been found to be approximately equal to the percentage increase in the average time interval, T_B, between two turbulent bursts.[26] Although the increase in the mean size of the streamwise eddies as seen from Fig. 6 provides indirect evidence for the increase in the streak spacing and hence in the time interval between the bursts, we present a quantitative picture based on the analyses of the energy spectra and the spatial correlation of the velocity below.

As seen in Fig. 8, the one-dimensional energy (Fourier) spectrum associated with the streamwise velocity fluc-

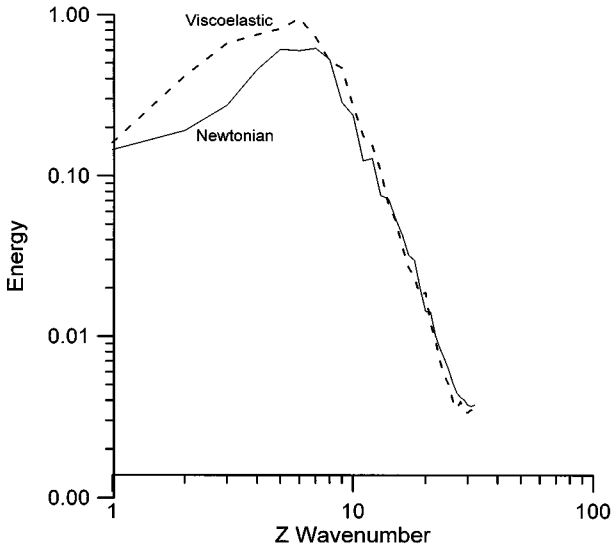

FIG. 8. The one-dimensional energy spectrum vs the spanwise wavenumber for the streamwise velocity fluctuations at $y=15$.

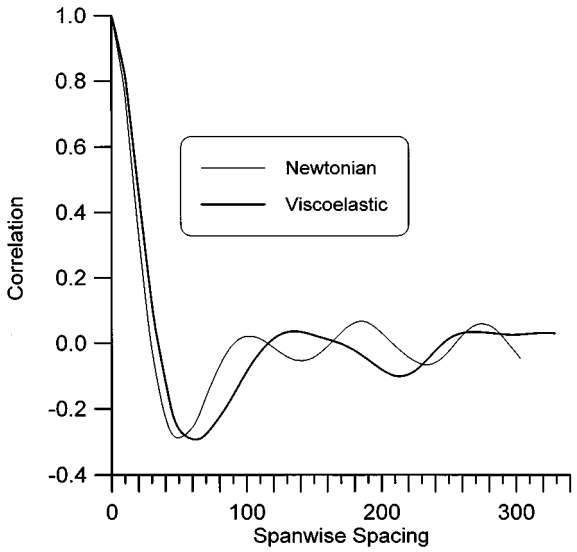

FIG. 9. The correlation of the streamwise fluctuating velocity as a function of spanwise spacing for both the Newtonian and viscoelastic flows.

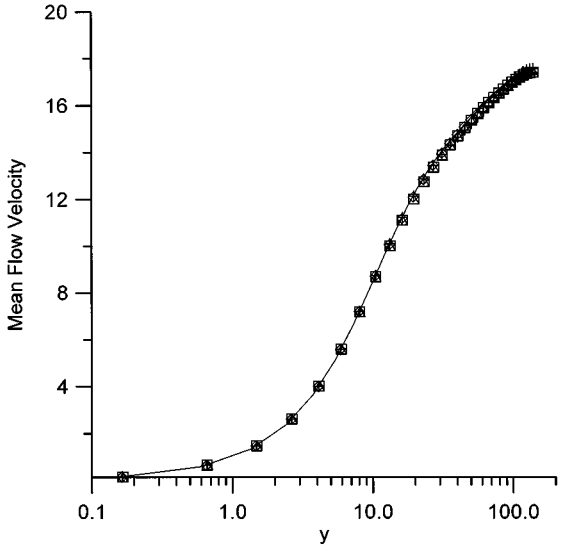

FIG. 10. $U(y)$ vs y for the Newtonian (solid line) and four viscoelastic flows ($L=2$) at $\mathrm{We}_\tau=12.5(\diamond)$, $25(+)$, $37.5(\square)$ and $50(\triangle)$.

tuations,[37] obtained from our simulation results, showed an increase in the energy contained in the low wavenumber (high wavelength) modes and a shift in the peak of the energy spectrum to a higher wavelength in the drag reduced flow, indicating an enhancement of the average streak spacing. By taking the Fourier transform of this spectrum, we obtained further quantitative evidence for this effect by calculating the correlation of the fluctuating streamwise velocity[37] as a function of spanwise spacing, Δz, for both the Newtonian and the viscoelastic flows. From these correlations, presented in Fig. 9, the average streak spacing can be evaluated as twice the distance between the z for which the correlation is a maximum (at $z=0$) and a minimum respectively. Our evaluation showed the increase in streak spacing to be approximately 30 viscous units, i.e., an increase from approximately 98 for the Newtonian to 128 for the viscoelastic. This is in very good agreement with the correlation of Tiederman,[63] which predicts $\Delta_s=28.5$ for 15% drag reduction.

C. Criteria for the onset phenomenon

In this section we would like to develop criteria for the onset of drag reduction based on our simulation results. In order to ascertain the effect of macromolecular extension and consequently the enhanced polymer resistance to flow deformation on drag reduction, we have performed a set of simulations using a low value of the parameter $L=2$, which corresponds to a maximum attainable value for the trace$(\tilde{\mathbf{c}})$ of 4 [note that the equilibrium chain conformation corresponds to trace$(\tilde{\mathbf{c}})=3$]. This change in the parameter L is important because, in conjunction with influencing the maximum extension of the polymer molecules, it also modifies the polymer resistance to extensional deformation. A measure of that resistance is provided by an analysis of the extensional viscosity, $\overline{\eta}$, defined for a homogeneous extensional flow as the ratio of the normal stress difference to the elongational rate, $\dot{\epsilon}$. For a Newtonian fluid, $\overline{\eta}$ is equal to three times the shear viscosity. The polymeric contribution to the total (solution) extensional viscosity, say $\overline{\eta_p}$, can be defined as

$$\overline{\eta_p}=\frac{\overline{\eta}-3\,\eta_s}{3\,\eta_{p0}}, \tag{9}$$

where $\overline{\eta}$ is evaluated as the ratio of the first normal stress difference and the elongational rate for the polymer solution.[52] As evident from Eq. (9), $\overline{\eta_p}$ approaches unity for low values of the elongational rate. For the FENE-P fluid, $\overline{\eta_p}$ as a function of $\lambda\dot{\epsilon}$ can be shown to undergo a sudden increase from 1 to a high viscosity plateau, say $\overline{\eta_{p\infty}}$, as $\lambda\dot{\epsilon}$ exceeds unity. It can be further shown that for $L=2$, $\overline{\eta_{p\infty}}$ remains practically unity, whereas for $L=10$, $\overline{\eta_{p\infty}}\approx 10$, for the value of the parameter $\beta=\eta_s/\eta_0=0.9$ used in our simulations [see Fig. 2 and Eq. (26) in Ref. 52]. For the FENE-P model, similar conclusions apply for the extensional viscosity in a biaxial extensional flow as well.[52]

The mean flow velocity profiles obtained from each one of the simulations performed for $L=2$ at $\mathrm{We}_\tau=12.5$, 25, 37.5 and 50 are presented in Fig. 10 along with the Newtonian flow profile. As can be seen from there, all the velocity profiles almost coincide indicating no detectable drag reduction. We found, consistent with these results, that the root mean square velocity statistics hardly deviated from the Newtonian flow results for all the four viscoelastic cases. These observations are consistent with a mechanism for drag reduction requiring a significantly enhanced extensional viscosity in the bulk of the flow resulting in the suppression of the eddies which carry the Reynolds stress in the buffer layer, as proposed in the past by Lumley,[23] Metzner and co-workers[20–22] and other investigators.[24,30,61] In particular, since the maximum attainable extensional viscosity value [$\overline{\eta_{p\infty}}$ achieved as $\lambda\dot{\epsilon}$ becomes $O(1)$] is a monotonically increasing function of L for the FENE-P fluid, a high enough value of L is necessary to achieve significant drag reduction. Moreover, as $\lambda\dot{\epsilon}$ increases, the response of the material to a *transient* extensional flow field becomes faster. In particular

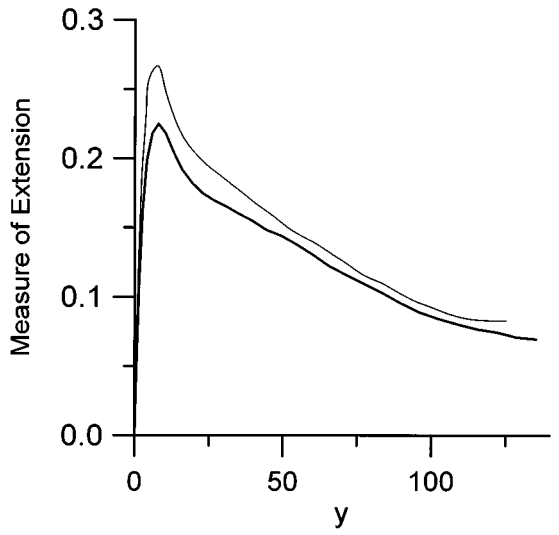

FIG. 11. $\dot{E}(y)$ [see Eq. (10)] in units of U_τ^2/ν_0 vs y in the Newtonian (thin line) and viscoelastic ($\mathrm{We}_\tau=50$, thick line) case.

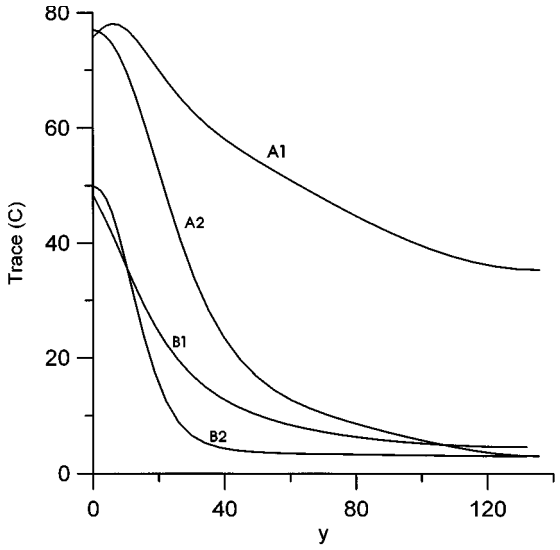

FIG. 12. Trace($\mathbf{C}$) vs y. Curve $A1$: $\mathrm{We}_\tau=50$ simulation result; Curve $A2$: $\mathrm{We}_\tau=50$, mean shear flow assumption; Curve $B1$: $\mathrm{We}_\tau=12.5$ simulation result; Curve $B2$: $\mathrm{We}_\tau=12.5$, mean shear flow assumption.

for the FENE-P model, it can be shown that the response of the fluid to transient extension is practically instantaneous if $\lambda\dot{\epsilon}\approx 5$ or greater.[52] These observations explain why drag reduction sets in rather abruptly, as an *onset* phenomenon.

In order to test the validity of this onset criterion we need to evaluate a characteristic extensional rate for the simulated turbulent flows. Given the complex, three-dimensional and time-dependent nature of the turbulent flow, this is not an easy task. Simple measures involving invariants of the rate of strain tensor, corrected for the local vorticity or rotation of the principal axes of the rate of strain tensor, have been proposed in the past.[64,65] However, such criteria were primarily developed for laminar and two-dimensional/axisymmetric flows and quite often could give misleading information for three-dimensional flow fields.[65] Recently, den Toonder *et al.*[43,44] have used the ratio of the third to the second invariant of the rate of strain tensor to characterize the extensional nature of a turbulent flow filed for pipe flows. This measure has the property that it reduces to the rate of extension for a uniaxial extensional flow field. However, for the planar extensional flow (as well as for any planar flow) the third invariant is zero and as such this criterion is not applicable. Given the planar nature of the mean flow in the channel flow geometry such a criterion is not used here. Instead, we opted to develop a measure which is closely connected with the production of vorticity in the flow due to stretching/squeezing of vortex elements, since the results presented in Sec. IV B 3 seem to suggest possible inhibition of such mechanisms due to viscoelasticity. Hence, we propose here a measure of extension $\dot{E}$ by considering the term representing the vortex stretching mechanism in the vorticity equation[37] defined as

$$\dot{E}(y)=\frac{\|\tilde{\mathbf{d}}\cdot\tilde{\omega}\|}{\|\tilde{\omega}\|}, \tag{10}$$

where $\tilde{d}_{ij}=(\partial\tilde{u}_i/\partial x_j+\partial\tilde{u}_j/\partial x_i)/2$ and $\|\mathbf{r}\|$ denotes the Euclidean norm of the vector quantity $\mathbf{r}$. Average values of $\dot{E}(y)$ are plotted as function of y in Fig. 11 for the Newtonian and the viscoelastic ($\mathrm{We}_\tau=50$, $L=10$) flows. It can be easily verified from there that although there is lower vortex stretching activity in the viscoelastic flow, a characteristic value for $\dot{E}(y)\nu_0/U_\tau^2$ in the buffer layer is approximately 1/4. This in turn implies from our simulations with $L=10$ that the onset of drag reduction which occurred for $12.5<\mathrm{We}_\tau\leqslant 25$ corresponds to $3<\lambda\dot{E}<7$, for that value of L. This result is consistent with the proposed criterion based on the response the FENE-P chains to transient extensional flow field.

In order to investigate further the connection between drag reduction and an enhanced resistance to deformation offered by the presence of polymer molecules in the flow, it is instructive to follow the average deformation of the molecules represented in the FENE-P model by the eigenvalues of the average conformation tensor $\mathbf{C}$. The magnitude of the sum of the eigenvalues of $\mathbf{C}\equiv\mathrm{trace}(\mathbf{C})$ is a measure of the molecular extension, which in turn gives rise to an enhanced normal stress value as evident from Eq. (2). Since extensional flows are particularly suitable in leading to high molecular extension and thereby to a substantial increase in the extensional viscosity, the presence of high molecular extension was often sought in previous investigations to signify both the presence of a strong extensional character of the flow and an increased polymer resistance to the flow. However, we would like to caution the reader here that even shear flows when they are strong enough can lead to appreciable molecular extension without signifying either an extensional flow character or an enhanced resistance of the fluid to the flow. Indeed, in most polymer systems under these circumstances one observes a reduction in the effective shear viscosity. Thus, large molecular extension is a *necessary*, but not a *sufficient* condition for the presence of a strong extensional flow character and data similar to those presented in

Fig. 11 should also be consulted simultaneously to evaluate an effective extensional rate.

In Fig. 12 we present trace($\mathbf{C}$) as a function of y obtained from the non-drag reducing ($\mathrm{We}_\tau = 12.5$, curve $B1$) and the drag reducing ($\mathrm{We}_\tau = 50$, curve $A1$) viscoelastic simulations using $L = 10$. Also presented in the same figure are the results obtained for the trace($\mathbf{C}$) using Eq. (5) and the mean velocity profile $U(y)$ obtained from the simulations: i.e., we use $U(y)$ and under the assumption of a mean shear flow, compute trace($\mathbf{C}$) using Eq. (5) and present them as well (curve $A2$ for $\mathrm{We}_\tau = 50$ and curve $B2$ for $\mathrm{We}_\tau = 12.5$) to compare with the results obtained for trace($\mathbf{C}$) from the simulations of the fully coupled problem. As can be seen from there, the molecular extension away from the wall (where from Fig. 11 a strong extensional character is evident) is much higher for the drag reducing case as compared to the non-drag reducing one. This is consistent with the cardinal role of the enhanced extensional viscosity proposed in this work. In contrast, next to the wall ($y < 5$), where the flow is shear dominated, the molecular extension is fairly high for both the cases; thus it can be accounted for by the trace($\mathbf{C}$) evaluated using the mean shear flow assumption. It can be further seen from Fig. 12 that *in the drag reducing case*, the profile for trace($\mathbf{C}$) obtained from the direct simulations is substantially different from those computed under the assumption of a mean shear flow, except very close to the wall. The shear flow assumption predicts practically no departure from the equilibrium value for trace($\mathbf{C}$) close to channel centerline, whereas in reality, the departure from the equilibrium conformation is a very well pronounced effect in the bulk of the flow, as seen from Fig. 12. On the other hand, for the non-drag reducing flow realized at $\mathrm{We}_\tau = 12.5$, the simulated profile and the one computed under a shear flow assumption can be seen to be in reasonably good agreement with each other.

Hence, the proposed criterion is based on the consideration that the ability of the macromolecule to achieve extension greater than a threshold value rapidly enough determines the onset of drag reduction. The ideas outlined in this section are not entirely novel ones, they have been used in the past by Lumley[2,3] to explain the onset phenomenon. The key difference between our line of reasoning and that of Lumley's ideas of molecular extension[2,3] is that the latter uses the (wall) flow time scale ν/U_τ^2 to identify an $O(1)$ We_τ for onset whereas we believe a more pertinent measure is obtained by using a quantity similar to $\dot{E}(y)$, leading to a critical Weissenberg number of order 10 for a dilute polymer solution.

D. Artificial stress diffusivity and mesh refinement

As mentioned in Sec. III, an artificial diffusive term was introduced into the evolution equation for the $\tilde{\mathbf{c}}$ tensor, i.e., Eq. (4), to stabilize the numerical calculations. The influence of the numerical diffusivity on the flow dynamics and stability was examined in detail in a previous work.[51] In addition, a detailed survey of the literature on the use of artificial diffusivity in numerical calculations of steady as well as time-dependent viscoelastic flows was also offered in that work.[51] As found from that work, the introduction of controlled amounts of numerical diffusivity such that $\kappa/(U_\tau)h \ll 1$, stabilizes the time-integration of Eq. (4) without altering appreciably the flow dynamics. Furthermore, if the magnitude of the diffusivity decreases at least linearly with the mesh size the results converge to those obtained with the original equation with mesh refinement.[66,67] In particular, in finite element formulations using the streamline upwinding (FE/SU) technique, one introduces an anisotropic (along the streamlines) tensorial diffusivity whose magnitude is proportional to the size of the element.[66] This diffusivity was found essential in order to stabilize the numerical algorithm, especially close to a singularity.[66] This issue has been very recently further explored by Purnode and Legat[68] in relation to the FENE-P fluid model used in this work. Using a FE/SU technique, they were able to obtain solutions in the flow through a sudden contraction at moderately high Reynolds numbers even under conditions under which there is a change of type of the equations.[68] Moreover, the achievement with the extensibility parameter (L) value of 10 of results very similar to those obtained with the highly extensible Oldroyd-B fluid (which is obtained from the FENE-P model in the limit of $L = \infty$) gives further justification for the use of the same value for L in this work.

We tested the convergence of the simulation results with respect to mesh refinement accompanied by a consistent reduction in the artificial diffusivity. Viscoelastic flow calculations were performed for $\mathrm{We}_\tau = 50$ and $L = 10$ with a finer mesh of $128 \times 129 \times 128$ and $\kappa = 5 \times 10^{-3} U_\tau h$ (this value of κ is half of that used for the $64 \times 65 \times 64$ mesh). The $128 \times 129 \times 128$ mesh translates to approximately 22 million variables and the CPU requirements per time step are approximately 10 times greater for this mesh as compared to the $64 \times 65 \times 64$ one. Hence, the computations were performed only for a shorter time interval of $6h/U_\tau$ time units (approximately 8 eddy turnover times) for the finer mesh. The input data for this set of simulations were obtained from the (suitably extrapolated) data for the $64 \times 65 \times 64$ mesh at $t = 56h/U_\tau$ (see also Fig. 1).

The results obtained for the viscoelastic flow for the two meshes are presented in Fig. 13 (for the average velocity) and Fig. 14 (rms fluctuations in the velocity). As it can be seen from these figures the results obtained with the two different mesh and artificial diffusivity values show the same qualitative behavior. Moreover, the small quantitative differences that exist can be attributed to a large part to the different input conditions used in the two simulations. In particular, from Fig. 13, it can be seen that the results for the larger mesh show a slightly higher drag reduction. Most of this difference should be attributed to the fact that the initial condition for this calculation corresponds to the interpolated data obtained with the coarser mesh at time $t = 56h/U_\tau$, i.e. at the end of the run shown in Fig. 1 corresponding to the maximum observed mean Reynolds number (and thus maximum drag reduction) which had still an increasing tendency and did not appear to have fully reached a stationary state. Moreover, it is important to notice from Fig. 14 that the changes seen in the rms statistics in the velocity components are *consistent* with the observation of higher drag reduction

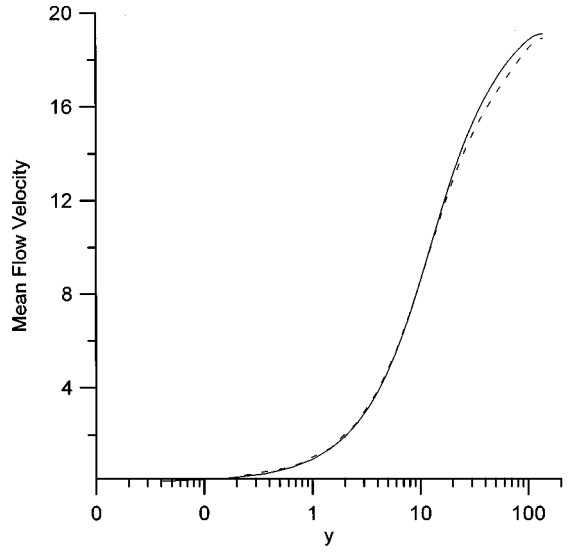

FIG. 13. Average velocity U as a function of y for the viscoelastic flow for $\mathrm{We}_\tau = 50$ and $L = 10$: $64 \times 65 \times 64$ mesh, $\kappa = 10^{-2} U_\tau h$ (dashed line); $128 \times 129 \times 128$ mesh, $\kappa = 5 \times 10^{-3} U_\tau h$ (solid line).

seen from Fig. 13 for the finer mesh, i.e., the streamwise velocity fluctuations are higher and the wall-normal and spanwise fluctuations are lower for the finer mesh which shows higher values of drag reduction. The self-consistency of the results is a further proof of the robustness of the simulations and the small if any effect of the artificial diffusivity in the conformation tensor evolution equation.

V. CONCLUSIONS

In this work we have successfully performed direct numerical simulations of the turbulent channel flow of a dilute polymer solution, using an independently evaluated rheological model, the FENE-P fluid model for the polymer chains. Although the Reynolds number used in the simulations was lower than that corresponding to the conditions under which drag reduction is experimentally observed with dilute polymer solutions, we were able to show that a reduction in the turbulent drag can be achieved if the viscoelasticity of the fluid model is sufficiently large. This is captured by allowing for a larger contribution of the polymer to the stresses ($\beta = 0.9$, corresponding to 10% contribution of the polymer to the total zero shear viscosity) as compared to the polymer solutions utilized in drag reduction experiments so far. Despite those limitations, the simulation results showed excellent qualitative agreement with the experimental observations associated with drag reduction both in the structural as well as in the statistical features of polymer-modified turbulence.

In particular, the simulations performed using $L = 10$ showed the ''onset'' phenomenon upon the satisfaction of a criterion, $12.5 < \mathrm{We}_\tau \leqslant 25$, which allows for sufficiently large extension of the polymer chains, contributing to an increased extensional viscosity. The statistical features of the drag-reduced turbulent flow, such as the root mean square velocity statistics, were shown to be in qualitative agreement with experimental observations wherever the latter are available. This is also supported by the numerical predictions for the increase in the average streak spacing associated with drag reduction. In particular, our simulation results have shown that the presence of viscoelastic forces results in a substantial reduction in the streamwise vorticity fluctuations. Since the quasi-streamwise vortices are known to play an important role in the production of turbulence, the observation of reduced rms streamwise vorticity seems to support a mechanism of drag reduction based on the inhibition of the turbulence generating events by the polymer chains. These observations led to the development of the aforementioned criterion for the onset of drag reduction by combining an analysis of the extensional flow characteristics based on our simulation results with the well-documented response of the FENE-P fluid model in steady as well as transient elongational flows.

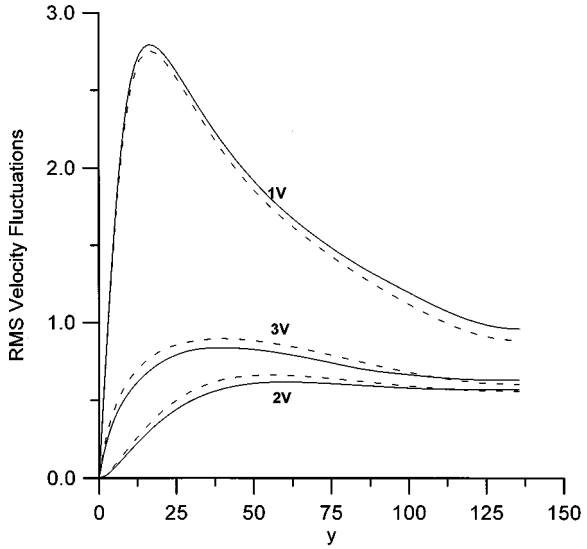

FIG. 14. Root mean square velocity fluctuations as a function of y for the viscoelastic flow for $\mathrm{We}_\tau = 50$ and $L = 10$: 1V, 2V and 3V denote the streamwise, wall-normal and spanwise components, respectively. $64 \times 65 \times 64$ mesh, $\kappa = 10^{-2} U_\tau h$ (dashed lines); $128 \times 129 \times 128$ mesh, $\kappa = 5 \times 10^{-3} U_\tau h$ (solid lines).

ACKNOWLEDGMENTS

The authors would like to acknowledge the financial support provided by NSF, Grant No. CTS-9114508 (R.S. and A.N.B.), by the graduate school of U. of Delaware through a competitive fellowship to R.S., and by the Office of Naval Research through the Fluid Dynamics Task Area at the Naval Research Laboratory (R.A.H.). We are grateful to the Pittsburgh Supercomputing Center for providing the computational resources used in this research. We would also like to acknowledge the use of computational facilities at the University of Delaware. A.N.B. would also like to acknowledge an ASEE/NAVY sabbatical leave fellowship and the ONR Grant No. N00014-94-1-0581. We express our thanks to professors Arthur Metzner and Abraham Lenhoff for their helpful comments and suggestions during the preparation of this article.

[1]B. A. Toms, ''Some observations on the flow of linear polymer solutions through straight tubes at large Reynolds numbers,'' Proceedings of the International Congress on Rheology, Vol. 2 (North Holland, Amsterdam, 1949), pp. 135–141.
[2]J. L. Lumley, ''Drag reduction by additives,'' Annu. Rev. Fluid Mech. **1**, 367 (1969).
[3]J. L. Lumley, ''Drag reduction in turbulent flow by polymer additives,'' J. Polymer Sci. Macromol. Rev. **7**, 263 (1973).
[4]P. S. Virk, ''Drag reduction fundamentals,'' AIChE J. **21**, 625 (1975).
[5]N. S. Berman, ''Drag reduction by polymers,'' Annu. Rev. Fluid Mech. **10**, 47 (1978).
[6]S. J. Kline, W. C. Reynolds, F. A. Schraub, and P. W. Runstadler, ''The structure of turbulent boundary layers,'' J. Fluid Mech. **30**, 741 (1967).
[7]H. P. Bakewell, Jr. and J. L. Lumley, ''Viscous sublayer and adjacent wall layer in turbulent pipe flow,'' Phys. Fluids **10**, 1880 (1967).
[8]E. R. Corino and R. S. Brodkey, ''A visual investigation of the wall region in turbulent flow, J. Fluid Mech. **37**, 1 (1969).
[9]H. T. Kim, S. J. Kline, and W. C. Reynolds, ''The production of turbulence near a smooth wall in a turbulent boundary layer,'' J. Fluid Mech. **50**, 133 (1971).
[10]G. L. Donohue, W. G. Tiederman, and M. M. Reischman, ''Flow visualization in the near-wall region in a drag reducing flow,'' J. Fluid Mech. **56**, 559 (1972).
[11]L. D. Eckelman, G. Fortuna, and T. J. Hanratty, ''Drag reduction and the wavelength of flow-oriented eddies,'' Nature Phys. Sci. **236**, 94 (1972).
[12]M. M. Reischman and W. G. Tiederman, ''Laser-Doppler anemometer measurements in drag-reducing channel flows,'' J. Fluid Mech. **70**, 369 (1975).
[13]D. K. Oldaker and W. G. Tiederman, ''Spatial structure of the viscous sublayer in drag-reducing channel flows,'' Phys. Fluids **20**, S133 (1977).
[14]B. U. Achia and D. W. Thompson, ''Structure of the turbulent boundary layer in drag reducing pipe flow,'' J. Fluid Mech. **81**, 439 (1977).
[15]W. G. Tiederman, T. S. Luchik, and D. G. Boggard, ''Wall-layer structure and drag reduction,'' J. Fluid Mech. **156**, 419 (1985).
[16]D. T. Walker and W. G. Tiederman, ''Turbulent structure in a channel flow with polymer injection at the wall,'' J. Fluid Mech. **218**, 377 (1990).
[17]G. Fortuna and T. J. Hanratty, ''The influence of drag-reducing polymers on turbulence in the viscous sublayer,'' J. Fluid Mech. **53**, 575 (1972).
[18]W. D. McComb and L. H. Rabie, ''Laser-Doppler measurements of turbulent structure,'' AIChE J. **28**, 558 (1982).
[19]H. Usui, M. Kodama, and Y. Sano, ''Laser-Doppler measurements of turbulence structure in a drag-reducing pipe flow with polymer injection,'' J. Chem. Eng. Jpn. **21**, 134 (1988).
[20]A. B. Metzner and M. G. Park, ''Turbulent flow characteristics of viscoelastic fluids,'' J. Fluid Mech. **20**, 291 (1964).
[21]F. A. Seyer and A. B. Metzner, ''Turbulence phenomena in drag-reducing systems,'' AIChE J. **15**, 426 (1969).
[22]A. B. Metzner, ''Polymer solution and fiber suspension rheology and their relationship to turbulent drag reduction,'' Phys. Fluids. **20**, S145 (1977).
[23]J. L. Lumley, ''Drag reduction in two phase and polymer flows,'' Phys. Fluids **20**, S64 (1977).
[24]H. W. Bewersdorff and N. S. Berman, ''The influence of flow-induced non-Newtonian fluid properties on turbulent drag reduction,'' Rheol. Acta **27**, 130 (1988).
[25]H. C. Hershey and J. L. Zakin, ''A molecular approach to predicting the onset of turbulent drag reduction in the turbulent flow of dilute polymer solutions,'' Chem. Eng. Sci. **22**, 1847 (1967).
[26]T. S. Luchik and W. G. Tiederman, ''Turbulent structure in low concentration drag-reducing channel flows,'' J. Fluid Mech. **190**, 241 (1988).
[27]R. B. Bird, C. F. Curtiss, R. C. Armstrong, and O. Hassager, *Dynamics of Polymeric Fluids* Vol. 1 (Wiley, New York, 1987).
[28]A. N. Beris and B. J. Edwards, *Thermodynamics of Flowing Systems with Internal Microstructure* (Oxford University Press, New York, 1994).
[29]M. J. Rudd, ''Velocity measurements made with a laser Dopplermeter on the turbulent pipe flow of a dilute polymer solution,'' J. Fluid Mech. **51**, 673 (1972).
[30]N. S. Berman, ''Flow time scales and drag reduction,'' Phys. Fluids. **20**, S168 (1977).
[31]P. G. de Gennes, ''Towards a scaling theory of drag reduction,'' Physica A **140**, 9 (1986).
[32]D. D. Joseph, *Fluid Dynamics of Viscoelastic Liquids* (Springer, New York, 1990).
[33]S. A. Orszag and L. C. Kells, ''Transition to turbulence in plane Poiseuille and plane Couette flow,'' J. Fluid Mech. **96**, 159 (1980).
[34]P. Moin and J. Kim, ''On the numerical solution of time-dependent viscous incompressible fluid flows involving solid boundaries,'' J. Comput. Phys. **35**, 381 (1980).
[35]J. Kim and P. Moin, ''Application of a fractional-step method to incompressible Navier-Stokes equations,'' J. Comput. Phys. **59**, 308.
[36]C. Canuto, M. Y. Hussaini, A. Quarteroni, and T. A. Zang, *Spectral Methods in Fluid Dynamics* (Springer, New York, 1988).
[37]H. Tennekes and J. L. Lumley, *A First Course in Turbulence* (MIT Press, Cambridge, MA, 1972).
[38]J. Kim, P. Moin, and R. Moser, ''Turbulence statistics in fully developed channel flow at low Reynolds number,'' J. Fluid Mech. **177**, 133 (1987).
[39]N. N. Mansour, J. Kim, and P. Moin, ''Reynolds-stress and dissipation-rate budgets in a turbulent channel flow,'' J. Fluid Mech. **194**, 15 (1988).
[40]R. A. Handler, E. Levich, and L. Sirovich, ''Drag reduction in turbulent channel flow by phase randomization,'' Phys. Fluids A **5**, 686 (1993).
[41]L. Sirovich, K. S. Ball, and L. R. Keefe, ''Plane waves and structures in turbulent channel flow, Phys. Fluids A **2**, 2217 (1990).
[42]L. Sirovich, K. S. Ball, and R. A. Handler, ''Propagating structures in wall bounded turbulent flows, Theor. Comput. Fluid Dyn. **2**, 307 (1991).
[43]J. M. J. den Toonder, Drag Reduction by Polymer Additives in a Turbulent Pipe Flow: Laboratory and Numerical Experiments, Ph.D. dissertation, Technische Universiteit Delft, 1995.
[44]J. M. J. den Toonder, F. T. M. Nieuwstadt, G. D. C. Kuiken, ''The role of elongational viscosity in the mechanism of drag reduction by polymer additives,'' Appl. Sci. Res. **54**, 95 (1995).
[45]P. Orlandi, ''A tentative approach to the direct simulation of drag reduction by polymers,'' J. Non-Newtonian Fluid Mech. **60**, 277 (1996).
[46]K. C. Porteus and M. M. Denn, ''Linear stability of plane Poiseuille flow of a viscoelastic liquids,'' Trans. Soc. Rheol. **16**, 295 (1972).
[47]R. Sureshkumar and A. N. Beris, ''Linear stability analysis of viscoelastic Poiseuille flow using an Arnoldi-based orthogonalization algorithm,'' J. Non-Newtonian Fluid Mech. **56**, 151 (1995).
[48]H. Massah, K. Kontomaris, W. R. Schowalter, and T. J. Hanratty, ''The configurations of a FENE bead-spring chain in transient rheological flows and in a turbulent flow,'' Phys. Fluids A **5**, 881 (1993).
[49]B. K. Maulik, Numerical Studies of the Oldroyd-B Fluid Stability and Transition in Planar Channels, Ph.D. dissertation, Princeton University, 1989.
[50]A. N. Beris and R. Sureshkumar, ''Simulation of time-dependent viscoelastic channel Poiseuille flow at high reynolds numbers,'' Chem. Eng. Sci. **51**, 1451 (1996).
[51]R. Sureshkumar and A. N. Beris, ''Effect of artificial stress diffusivity on the stability of numerical calculations and the dynamics of time-dependent viscoelastic flows,'' J. Non-Newtonian Fluid Mech. **60**, 53 (1995).
[52]L. E. Wedgewood and R. B. Bird, ''From molecular models to the solution of flow problems,'' Ind. Eng. Chem. Res. **27**, 1313 (1988).
[53]L. G. Leal, ''Dynamics of dilute polymer solutions,'' in *Structure of Turbulence and Drag Reduction* (Springer, New York, 1990), pp. 155–185.
[54]R. Sureshkumar and A. N. Beris, *Parallelization of a Spectral Method for Turbulent Flow Calculations*, AIChE 1995 National Meeting, Miami Beach, Florida (1995).
[55]R. B. Bird, C. F. Curtiss, R. C. Armstrong, and O. Hassager, *Dynamics of Polymeric Fluids* Vol. 2 (Wiley, New York, 1987).
[56]A. Peterlin, ''Streaming birefringence of soft linear macromolecules with finite chain length,'' Polymer **2**, 257 (1961).
[57]P. S. Bernard, J. M. Thomas, and R. A. Handler, ''Vortex dynamics and the production of Reynolds stress,'' J. Fluid Mech. **253**, 385 (1993).
[58]R. Dean, ''Reynolds number dependence of skin friction and other bulk flow quantities in two-dimensional rectangular duct flow,'' Trans. ASME I: J. Fluids Eng. **100**, 215 (1978).
[59]F. T. Pinho and J. H. Whitelaw, ''Flow of non-Newtonian fluids in a pipe,'' J. Non-Newtonian Fluid Mech. **34**, 129 (1990).
[60]W. W. Wilmarth, T. Wei, and C.O. Lee, ''Laser anemometer measurements of Reynolds stress in a turbulent channel flow with drag reducing polymer additives, Phys. Fluids **30**, 933 (1987).
[61]A. Gyr and H. W. Bewersdorff, ''Change of structures close to the wall of a turbulent flow in drag reducing fluids,'' in *Structure of Turbulence and Drag Reduction* (Springer, New York, 1989), pp. 215–222.
[62]J. W. Brooke and T. J. Hanratty, ''Origin of turbulence producing eddies in a channel flow,'' Phys. Fluids A **5**, 1011 (1993).

[63]W. G. Tiederman, ''The effect of dilute polymer solution on viscous drag and turbulence structure,'' in *Structure of Turbulence and Drag Reduction* (Springer, New York, 1990), pp. 187–200.
[64]G. Astarita, ''Objective and generally applicable criteria for flow classification,'' J. Non-Newtonian Fluid Mech. **6**, 69 (1979).
[65]R. R. Huilgol, ''Comments on 'Objective and generally applicable criteria for flow classification' by G. Astarita,'' J. Non-Newtonian Fluid Mech. **7**, 91 (1980).
[66]M. J. Crochet and V. Legat, ''The consistent streamline-upwind/Petrov-Galerkin method for viscoelastic flow revisited,'' J. Non-Newtonian Fluid Mech. **42**, 283 (1992).
[67]V. Legat and J. M. Marchal, ''On the stability and accuracy of fully coupled finite element techniques used to simulate the flow of differential viscoelastic fluids: A one-dimensional model,'' J. Rheol. **36**, 1325 (1992).
[68]B. Purnode and V. Legat, ''Hyperbolicity and change of type in flows of FENE-P fluids,'' J. Non-Newtonian Fluid Mech. **65**, 111 (1996).